Desalination and Water Treatment
www.deswater.com

doi: 10.5004/dwt.2022.28559

264 (2022) 111–120
July

Effect of pH on the adsorptive and cycling performance of amphoteric clay-loaded biochar

Wen-bin Li[a], Hong-yan Deng[a,*], Yong Ye[a,*], Shu-ni Zhou[a], Abbas Touqeer[b], Jiang-ming Ouyang[a], Qi Kuang[a], Wei Liu[c]

[a]*College of Environmental Science and engineering, China West Normal University, Nanchong Sichuan 637009, China, Tel. +86 08172568646; emails: dhongyan119@163.com (H.-y. Deng), 1574423101@qq.com (Y. Ye), lwb062@163.com (W.-b. Li), 3234017295@qq.com (S.-n. Zhou), jaihsiuhiasu.111@qq.com (J.-m. Ouyang), 1725190516@qq.com (Q. Kuang)*
[b]*Department of Soil, Water, and Climate, University of Minnesota, Twin 637009, USA, email: abbastouqeer@yahoo.com (A. Touqeer)*
[c]*School of Chemical and Environmental Engineering, Xinjiang Institute of Engineering, Urumqi 830091, China, email: lwmjp@163.com (W. Liu)*

Received 5 February 2022; Accepted 11 May 2022

ABSTRACT

To investigate the effect of solution pH on the adsorption and reuse of carbon-based composites, xerophilic and hydrophytic *Alternanthera philoxeroides* biochars (XAp-C and HAp-C) were loaded with 0%, 50%, and 100% dodecyl dimethyl betaine (BS-12)-modified bentonite (B, 50BS-B, and 100BS-B) to form Ap-C/B, Ap-C/50BS-B, and Ap-C/100BS-B, respectively. Then, the isothermal adsorption and morphological changes of Cu^{2+} and cycling performance by the tested materials under different pH gradients were studied with XAp-C and HAp-C as the control. Results revealed the following. (1) The adsorption isotherms of Cu^{2+} for the tested materials were all consistent with the Langmuir model, and the maximum adsorption amount remained between 100.82–286.31 mmol/kg. Under the same conditions, the adsorption amount of XAp-C/BS-B was better than that of HAp-C/BS-B, and that of XAp-C/100BS-B was the best. (2) Thermodynamic parameter analysis showed that Cu^{2+} adsorption of the tested materials was a spontaneous, endothermic, and entropy-increasing reaction process. Kinetic fitting further showed that Cu^{2+} adsorption conformed to the pseudo-second-order kinetic model. (3) Within pH 2–6, the amount of Cu^{2+} adsorbed onto the tested materials all initially increased and then decreased, and the value at pH 5 was the best. (4) The Cu adsorbed onto the tested materials primarily existed in exchangeable and organic matter forms, followed by the carbonate form and then the Fe–Mn oxide form. With increased pH, Cu in carbonate form gradually transformed into the organic matter form, whereas Cu in exchangeable and Fe–Mn oxide forms remained basically unchanged. In summary, using XAp-C/100BS-B and adjusting the pH to 5 was the most favorable for Cu^{2+} adsorption, and the adsorption amount was 62.6% of the raw material after three times of regeneration.

Keywords: Biochar; Amphoteric bentonite; Cu^{2+} adsorption; Morphology; Cycling performance

1. Introduction

With the development of industrialization and urbanization, the soil-environment pollution by heavy metals has become particularly prominent [1,2]. The migration, bioavailability, and harmfulness of heavy metals in soil are related to the total amount of heavy metals and to a greater extent on the heavy-metal forms [3]. Currently,

* Corresponding authors.

soil remediation focuses on the adsorption and fixation method by using soil amendments [4]. However, how to control the total pollution of heavy metals with efficient adsorption materials and deeply analyze the characteristics of their morphological changes are the difficulties and hotspots of current research [5–7].

The materials commonly used to absorb heavy metals include activated carbon, activated sludge, clay, agricultural and forestry wastes, etc. [8,9]. Bentonite (B) and biochar (C) are excellent adsorbents, cheap and easy to obtain, and extensively used. However, heavy metals adsorbed onto B are prone to desorption, and C is susceptible to pH changes. In practice, B and C are often modified to enhance the adsorption effect of heavy metals [10,11]. The commonly used modifiers are surfactants, inorganic modifiers, and natural small-molecule acids. Li et al. [12] modified bamboo and coconut shell C by using cetyltrimethyl ammonium bromide (CTAB), and the saturated adsorption capacity of CTAB-modified C to Cd^{2+} is 12.56 and 10.71 mg/g, respectively. Modification of C by inorganic modifier ($KMnO_4$) increases the adsorption capacity of C to Cd^{2+} by more than seven times [13]. Amphoteric surfactant has positive and negative charges at the hydrophilic end and also contains carbon chains at the hydrophobic end [14,15]. With the unique molecular structure of amphoteric surfactant, we could realize the simultaneous adsorption of organic and heavy-metal pollutants [16]. When B is modified by the amphoteric surfactant dodecyl dimethyl betaine (BS-12), the maximum adsorption capacity of Cu^{2+} and Pb^{2+} by BS-12-modified B (BS-B) is 2.9%–56.3% and 13.1%–31.8% higher, respectively, than that by B [17]. After simultaneous modification by BS-12 and I-decane sodium sulfonate (DAS), the adsorption capacity of BS-12+DAS-modified B for Cr^{6+} and Cd^{2+} is 2.4–9.7 times higher than that of B. The adsorption capacity of B for heavy metals reaches the maximum under modification with BS-12 and DAS [18]. The performance of adsorbed materials cannot be well characterized only from the level of adsorption capacity, and the migration and morphology of heavy metals in materials require further analysis [19,20]. Studies have shown that the forms of heavy metals in different environmental media are complex, and that the content and proportion of different forms heavy metals greatly differ [21]. Investigating the adsorption capacity and morphological change can well characterize the performance differences among adsorbed materials.

As one of the first invasive species in China, *Alternanthera philoxeroides* has strong growth ability and wide geographical distribution, seriously endangering the development of social economy and ecological environment. If *Alternanthera philoxeroides* is made into C (hereafter denoted as Ap-C), then a new type of composite adsorption material could be prepared by combining Ap-C with BS-B. It solves the problem of biomass resource waste of invasive species and confers the composite material with the advantages of Ap-C and BS-B. Few studies have been reported about this aspect so far. In the present study, different BS-B-loabed Ap-C samples were taken as the research object. The isothermal-adsorption characteristics of Cu^{2+} onto each composite material under the major environmental factors (pH) were analyzed, and the morphological changes of Cu were compared. The aim of this study was to reduce the harm of biological invasion and provide a theoretical basis for the preparation and application of environmental materials.

2. Materials and methods

2.1. Experimental materials

BS-12 was used as an amphoteric modifier (AR grade; produced by Tianjin Xingguang Auxiliary Factory, Tianjin City, China). The molecular formula of BS-12 is $C_{16}H_{33}NO_2$, and its pH is 6.5–7.5. The solubility (20°C) is 160 g/100 g water, and the active substance content is 50% ± 2%. B (particle size of 400 mesh) was purchased from Xinyang City, China and purified by washing before use. The basic physico-chemical properties of B after purification were as follows: cation exchange capacity (CEC), 1,000.33 mmol/kg; pH, 9.59; and total organic carbon, 4.98 g/kg. Then, 0%, 50%, and 100% BS-B (denoted as B, 50BS-B, 100BS-B, respectively) were prepared by wet method [22].

The biomass of xerophilic (X) and hydrophytic (H) *Alternanthera philoxeroides* was used to prepare two Ap-C samples. The collected *Alternanthera philoxeroides* samples were washed with deionized water, dried in a 105°C blast-drying oven to constant weight, crushed, and placed in a muffle furnace under the protection of nitrogen for pyrolysis (400°C for 2 h). After pyrolysis time ended, XAp-C and HAp-C were obtained by passing through a 60-mesh sieve.

BS-B-loaded Ap-C materials were prepared by the following method. A total of 10 g of B (or BS-B) was placed in a 1 L glass container (0.5 L of deionized water) by ultrasonic dispersion and shaken at constant temperature for 6 h at 150 rpm. After adding 100 g of C (XAp-C or HAp-C), the mixture was continually shaken at constant temperature for 12 h. The supernatant was obtained after centrifuging, and then the bottom product was dried at 60°C and passed through a 60-mesh sieve. The four different BS-B-loaded Ap-C materials obtained were XAp-C/B (XAp-C loaded with B, the same as the rest materials), XAp-C/50BS-B, XAp-C/100BS-B, HAp-C/B, HAp-C/50BS-B, and HAp-C/100BS-B. Table 1 shows the basic physico-chemical properties of the different materials.

Table 1
Basic physico-chemical properties of the tested materials

Tested sample	pH	Cation exchange capacity (mmol/kg)	Specific surface area (m^2/g)
XAp-C	9.20	168.22	11.42
XAp-C/B	9.51	332.17	16.34
XAp-C/50BS-B	9.06	225.33	11.45
XAp-C/100BS-B	8.37	141.55	7.18
HAp-C	8.94	152.01	8.27
HAp-C/B	9.10	219.39	7.17
HAp-C/50BS-B	8.52	188.46	5.73
HAp-C/100BS-B	7.84	116.68	4.51

2.2. Experimental design

2.2.1. Cu^{2+} concentration gradient setting

The preliminary experiment showed that the adsorption isotherm began to turn when the concentration of Cu^{2+} is 300–400 mg/L. Therefore, nine concentration gradients of Cu^{2+} were set as 0, 20, 50, 100, 150, 200, 300, 400 and 500 mg/L. The adsorption isotherm experiments were carried out at 20°C and 40°C, respectively, with 3 replicates for each treatment.

2.2.2. Influence of pH on Cu^{2+} adsorption

pH Vis an important environmental factor to determine the existing form of heavy metals, and largely determines the protonation process of functional groups on the surface of the medium. Comprehensive consideration of the actual environment and application conditions, the pH of the initial solution was set to 2, 3, 4, 5, and 6. Each treatment was repeated thrice.

2.2.3. Adsorption kinetics of Cu^{2+}

A 500 mg/L Cu^{2+} solution was prepared, placed in multiple 50 mL centrifugal tubes. Add 0.5000 g composite materials respectively. The concentrations of Cu^{2+} were sampled for 0, 0.2, 1, 1.5, 2, 4, 6, 8, 10, 12, 16, 20, 24, 30, 36, 42, 48 and 60 h, respectively.

2.3. Experimental methods

2.3.1. Isothermal adsorption of Cu^{2+}

A total of 0.5000 g of samples was weighed in nine 50 mL plastic centrifuge tubes, and 20.00 mL of an Cu^{2+} solution with different concentration gradients were added to the pipette under optimal environmental conditions (150 rpm and 12 h oscillation). The equilibrium adsorption of Cu^{2+} in the supernatant was determined through centrifugation at 4,800 rpm for 20 min, the equilibrium adsorption amount of Cu^{2+} was determined, and the equilibrium adsorption amount of each material was calculated through subtraction. The influence of pH on Cu^{2+} adsorption was obtained by repeating the above process under different pH of the initial solution.

2.3.2. Morphological changes of Cu^{2+}

The materials obtained after adsorption of 500 mg/L Cu^{2+} were analyzed by the Tessier five-step extraction method for the content of various forms of Cu [19]. The Cu^{2+} content was determined by flame atomic-absorption spectrophotometry, and background absorption was corrected through the Zeeman effect.

2.4. Data processing

2.4.1. Fitting of adsorption isotherms

The Langmuir isotherm model was selected on the basis of the adsorption isotherm trend [16], and the isothermal equation [Eq. (1)] is as follows:

$$q = \frac{q_m bc}{1+bc} \tag{1}$$

where q_m indicates the maximum adsorption amount of Cu^{2+} on the different materials, mmol/kg; b represents the apparent equilibrium constant of the Cu^{2+} adsorption, which can be used to measure the affinity of adsorption.

2.4.2. Calculation of thermodynamic parameters

Parameter b in the Langmuir model is equivalent to the apparent adsorption constant of equilibrium constant, and the thermodynamic parameter calculated by $b = K$ was called the apparent thermodynamic parameter; Eqs. (2)–(4) were defined as follows:

$$\Delta G = -RT\ln K \tag{2}$$

$$\Delta H = R\left(\frac{T_1 \cdot T_2}{T_2 - T_1}\right)\cdot \ln\left(\frac{K, T_2}{K, T_1}\right) \tag{3}$$

$$\Delta S = \frac{\Delta H - \Delta G}{T} \tag{4}$$

where ΔG is the standard free energy change (kJ/mol), R is a constant (8.3145 J/mol/K), T is the adsorption temperature (T_1 = 293.16 K, T_2 = 313.6 K), ΔH is the enthalpy of adsorption process (kJ/mol), and ΔS is the entropy change of adsorption process (J/mol/K).

2.4.3. Calculation of kinetic parameters

The adsorption amount at different time were fitted by pseudo-first-order [Eq. (5)] and pseudo-second-order [Eq. (6)] kinetic models, respectively.

$$q_t = q_e\left(1 - e^{-k_1 t}\right) \tag{5}$$

$$q_t = \frac{k_2 q_e^2 t}{1 + k_2 q_e t} \tag{6}$$

where q_e is the equilibrium adsorption amount (mmol/kg); q_t is the adsorption capacity at t (min) (mmol/kg); k_1 and k_2 are pseudo-first-order and pseudo-second-order kinetic constants, respectively.

CurveExpert 1.4 fitting software was used in isothermal fitting, SPSS 16.0 statistical analysis software was used to process the experimental data for variance and correlation analysis, and Origin 9.0 software was adopted to improve data plotting.

3. Results and analysis

3.1. Isothermal adsorption characteristics of Cu^{2+} by the tested materials

Fig. 1 shows that all tested materials maintained a high adsorption capacity for Cu^{2+}. With increased equilibrium

concentration, the adsorption capacity of the tested materials for Cu^{2+} gradually increased and finally reached the adsorption saturation, generally presenting an "L" shape. The Cu^{2+}-adsorption capacity ranked in the order of Ap-C/100BS-B > Ap-C/50BS-B > Ap-C/B > Ap-C under the same equilibrium concentration. Under the maximum concentration gradient of Cu^{2+}, the adsorption rates of different tested materials all exceeded 60%. Furthermore, no significant difference existed in the adsorption rate of Cu^{2+} between XAp-C/BS-B and HAp-C/BS-B. The adsorption rate of Cu^{2+} showed the same trend as its adsorption capacity. The average adsorption rates of Ap-C/100BS-B were all nearly 90%, which was about 1.5 times higher than that of Ap-C.

The Langmuir adsorption isotherm equation was used for curve-fitting analysis, and the result parameters are shown in Table 2. The correlation coefficient (r values) all exceeded 0.98 and reached very significant level ($P < 0.01$), indicating that the Langmuir model suitably described Cu^{2+} adsorption onto the tested materials. The maximum adsorption capacity (q_m) of Cu^{2+} on the tested materials changed between 100.82 and 286.31 mmol/kg and decreased in the order XAp-C/100BS-B > HAp-C/100BS-B > XAp-C/50BS-B > HAp-C/50BS-B > XAp-C/B > HAp-C/B > XAp-C > HAp-C. The q_m values of Cu^{2+} on XAp-C/100BS-B, XAp-C/50BS-B, and XAp-C/B were 2.12, 1.78, and 1.48 times higher than that on XAp-C, whereas the q_m values of Cu^{2+} on HAp-C/100BS-B, HAp-C/50BS-B, and HAp-C/B were 1.31–2.04 times higher than that on HAp-C. These results indicated that loading BS-B can remarkably improve the adsorption performance of Cu^{2+} on Ap-C, and that a higher modification proportion of BS-12 on BS-B resulted in stronger Cu^{2+}-adsorption capacity of Ap-C/BS-B. Moreover, the q_m of Cu^{2+} on XAp-C/BS-B was 7.22%–21.08% higher than that on XAp-C/BS-B under the same loading condition. The average adsorption rate of Cu^{2+} on each tested material exceeded 60% and reached the peak value of 91.19 on XAp-C/100BS-B. The affinity constant b of each tested material for Cu^{2+} adsorption remained within 1.01–4.66, indicating weak adsorption affinity.

3.2. Thermodynamic and kinetic characteristics of Cu^{2+} adsorption

Under the conditions of 20°C and 40°C, Table 3 shows the results of the thermodynamic parameters of Cu^{2+} adsorption

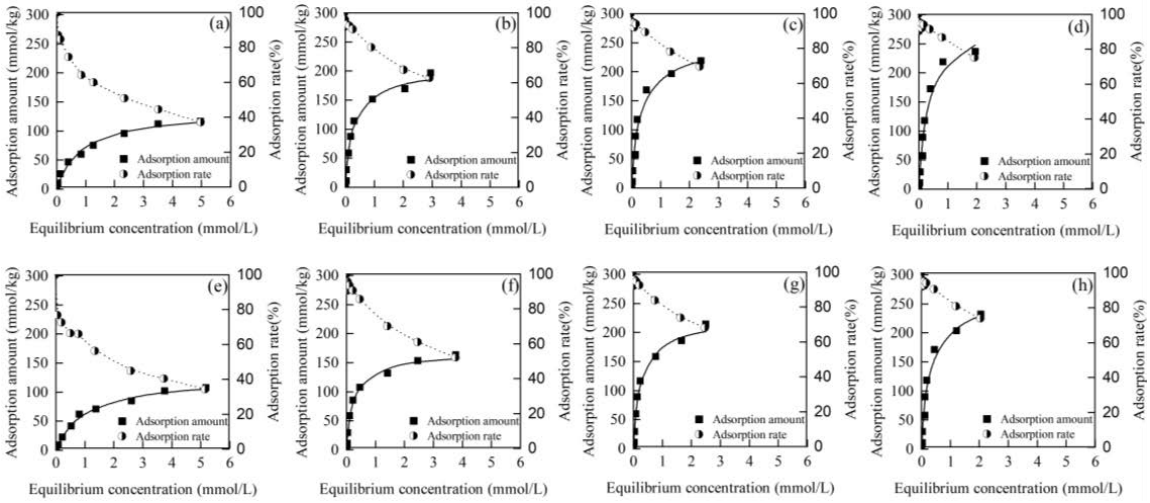

Fig. 1. Adsorption isotherms of Cu^{2+} on XAp-C (a), XAp-C/B (b), XAp-C/50BS-B (c), XAp-C/100BS-B (d), HAp-C (e), HAp-C/B (f), HAp-C/50BS-B (g), and HAp-C/100BS-B (h).

Table 2
Langmuir fitting parameters of Cu^{2+} adsorption isotherms

Tested material	Correlation coefficient (r)	Standard deviation (S)	q_m (mmol/kg)	b	Average adsorption rate (%)
XAp-C	0.9923**	5.70	135.07	1.16	67.00
XAp-C/B	0.9948**	7.78	199.80	4.22	86.15
XAp-C/50BS-B	0.9905**	12.02	240.43	4.10	89.52
XAp-C/100BS-B	0.9897**	13.59	286.31	3.32	91.19
HAp-C	0.9961**	3.75	125.98	1.01	62.02
HAp-C/B	0.9939**	7.21	165.02	4.66	82.10
HAp-C/50BS-B	0.9935**	9.51	217.94	4.83	88.51
HAp-C100BS-B	0.9913**	12.05	257.20	4.03	90.69

**indicates significance at the $p = 0.01$ level ($r = 0.765$ at $p = 0.01$ when the degrees of freedom $f = 8$).

by the tested materials. The apparent free-energy change (ΔG) of Cu^{2+} adsorption at 20°C and 40°C was negative, indicating that Cu^{2+} adsorption onto all tested materials was spontaneous. The ΔG values in the same soil samples were $-\Delta G_{40°C} > -\Delta G_{20°C}$, indicating that increased temperature enhanced the spontaneity of antibiotic adsorption. The apparent enthalpy change (ΔH) values of Cu^{2+} adsorption onto the tested materials were all positive, indicating that Cu^{2+} adsorption was endothermic and that increasing the temperature enhanced the adsorption. The ΔS values of the tested materials were positive, indicating that the surface disorder of adsorption system was large. Cu^{2+} adsorption onto the tested materials was a spontaneous, endothermic, and entropy-increasing process.

Fig. 2 shows the profile and trend of the tested materials' Cu^{2+}-adsorption kinetic curves. In the first 4 h of Cu^{2+} adsorption, the amount of Cu^{2+} adsorbed onto the tested materials increased rapidly, indicating that the adsorption rate was fast and it was a rapid adsorption stage. About 4 h later, the adsorption kinetic curves gradually flattened, and the adsorption amount of Cu^{2+} increased slightly with time. This stage was considered as close to equilibrium. The pseudo-first- and pseudo-second-order dynamic models were used to simulate the adsorption kinetic curves of Cu^{2+}, and the parameters are shown in Table 4. For the same material, the *R*-square (R^2) fitted by the pseudo-second-order kinetic model was higher than that by the pseudo-first-order kinetic model, and the theoretical value of equilibrium adsorption amount (q_e) calculated by the pseudo-second-order kinetic equation was closer to the experimental result. Accordingly, the process of Cu^{2+} adsorption onto the tested materials was in accordance with the pseudo-second-order kinetic mechanism, and the adsorption rate of Cu^{2+} was proportional to the square of the driving force rather than directly proportional to the driving force. The adsorption rate was controlled by chemisorption mechanism, consistent with the thermodynamic parameters.

3.3. Influence of pH on Cu^{2+} adsorption onto the tested materials

Fig. 3 shows the influence trend of pH on the Cu^{2+} adsorption ability of each tested material. Within pH 2–6, the amount of Cu^{2+} adsorbed onto the tested materials initially increased and then decreased with increased pH and reached the maximum at pH 5. With increased pH from 2 to 5, the increase rate of Cu^{2+}-adsorption amount was 8.85%–24.48%, and decreased in the following order: HAp-C

Table 3
Thermodynamic parameters of Cu^{2+} adsorption

Tested material	20°C			40°C		
	ΔG (kJ/mol)	ΔH (kJ/mol)	ΔS (J/mol/K)	ΔG (kJ/mol)	ΔH (kJ/mol)	ΔS (J/mol/K)
XAp-C	–17.20	1.92	65.23	–18.50	1.92	65.23
XAp-C/B	–20.35	7.53	95.08	–22.25	7.53	95.08
XAp-C/50BS-B	–20.27	2.69	78.35	–21.84	2.69	78.35
XAp-C/100BS-B	–19.76	3.82	80.45	–21.37	3.82	80.45
HAp-C	–16.86	3.95	70.97	–18.28	3.95	70.97
HAp-C/B	–20.59	2.61	79.1	–22.17	2.61	79.13
HAp-C/50BS-B	–20.67	1.55	75.81	–22.19	1.55	75.81
HAp-C100BS-B	–20.23	4.21	83.38	–21.90	4.21	83.38

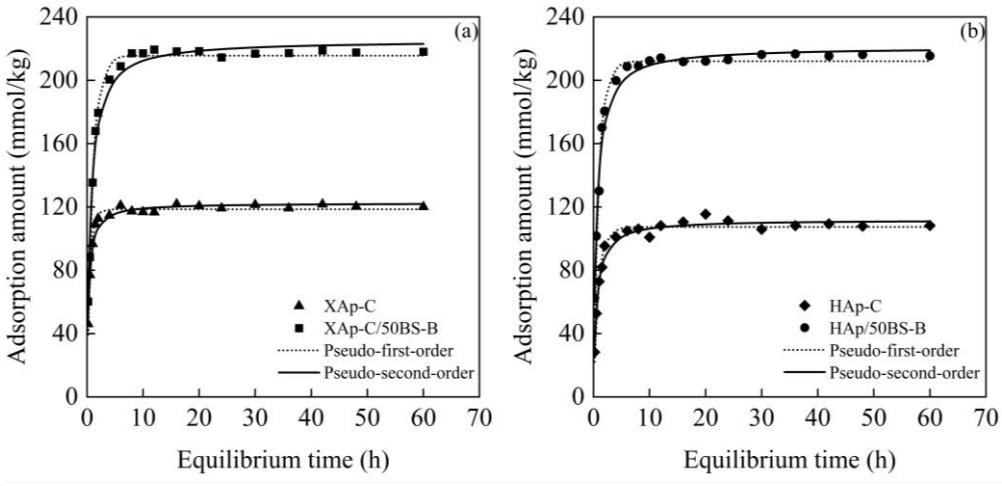

Fig. 2. Fitting curves by adsorption kinetic models of XAp-C/BS-B (a) and HAp-C/BS-B (b).

Table 4
Fitting parameters of adsorption kinetic curves of Cu^{2+}

Tested material	Actual adsorption amount (mmol/kg)	Adsorption kinetic model					
		Pseudo-first-order			Pseudo-second-order		
		q_e (mmol/kg)	k_1	R^2	q_e (mmol/kg)	k_2	R^2
XAp-C	121.66	118.57	2.0115	0.9861	122.40	0.0291	0.9895
XAp-C/50BS-B	223.35	215.58	1.0188	0.9908	225.18	0.0074	0.9925
WAp-C	110.24	107.33	1.1597	0.9839	111.89	0.0171	0.9898
WAp-C/50BS-B	219.11	212.01	1.1053	0.9862	220.91	0.0084	0.9937

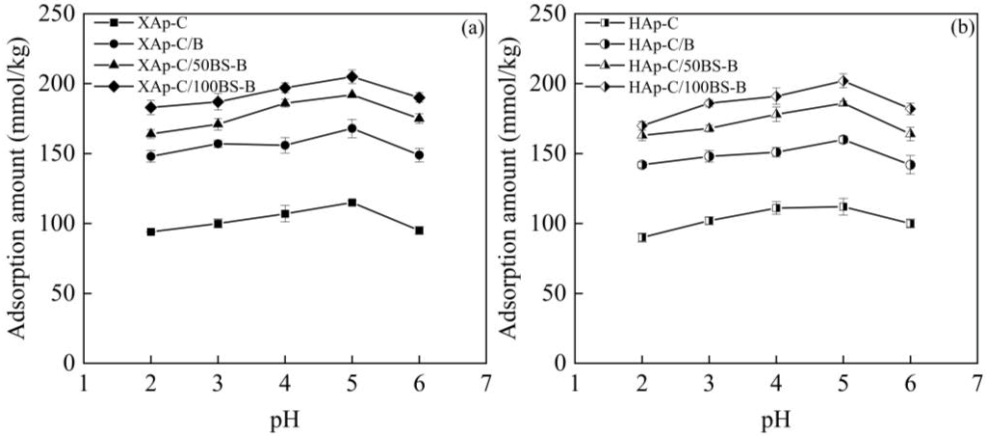

Fig. 3. Effect of pH on Cu^{2+} adsorption amount.

(24.48%) > XAp-C (23.00%) > HAp-C/100BS-B (18.59%) > XAp-C/50BS-B (14.15%) > HAp-C/50BS-B (14.15%) > XAp-C/B (13.59%) > HAp-C/B (12.59%) > XAp-C/100BS-B (12.39%). These results indicated that the adsorption stability of Cu^{2+} on Ap-C/BS-B improved compared with that of raw Ap-C, and the influence of pH on Ap-C/BS-B gradually decreased. XAp-C/100BS-B had the most stable performance for adsorbing Cu^{2+} among the tested materials.

At low pH, the Si–O^- and Al–O^- groups in the adsorbed material were protonated due to pH < pH_{PZC} (point of zero charge), and the electric potential gradually changed from negative to positive. Mutual repulsion with Cu^{2+} existed in the solution, leading to reduced electrostatic gravitational interaction with Cu^{2+} [23]. Additionally, the H^+ content in the solution was considerably higher than that of Cu^{2+} at low pH, and the surface of the material was covered by H^+, which played a dominant role in the competition with Cu^{2+} and other cations for the adsorption site on the material surface. Consequently, the Cu^{2+} content that can be absorbed by the material decreased. With increased pH, the competitive adsorption decreased and the cations in the solution were primarily Cu^{2+}. Meanwhile, the electronegativity of the material gradually strengthened, prompting the negatively charged adsorption sites on the material surface to combine with Cu^{2+}, and thus increased the Cu^{2+} adsorption amount. Moreover, a small increase in OH^- can partially combine with Cu^{2+} to form precipitates, which were bound to the material surface through complexation. However, at pH > 5, OH^- in the solution competed with OH^- on the material surface, resulting in decreased amount of Cu^{2+} adsorbed by the material. Therefore, the optimum effect was achieved at pH 5 in the experiment.

3.4. Distribution of Cu forms on the tested materials

The distribution of Cu forms adsorbed onto the tested materials is shown in Fig. 4. The proportion of Cu forms on the surface of each material showed a trend of organic matter form > exchangeable form > carbonate form > iron-manganese oxide form. The Fe–Mn oxide form accounted for the smallest proportion of Cu in all materials, which did not exceed 10% of the total copper amount. Organic matter form accounted for more than 50% of the total Cu in the tested materials (except HAp-C/100BS-B). Compared with Ap-C, the proportion of Cu in carbonate form adsorbed onto Ap-C/BS-B increased, whereas that in exchangeable form adsorbed onto Ap-C/BS-B decreased. Compared with HAp-C/BS-B, XAp/BS-B adsorbed a higher content of carbonate form of Cu. Overall, Cu in organic matter and exchangeable forms accounted for the largest proportion of Cu adsorbed onto the tested materials, and the total proportion exceeded 70%.

3.5. Influence of pH on the contents of Cu forms

The changes in content of various Cu forms on the tested materials are shown in Fig. 5. The Cu content of the tested materials in the same forms all decreased in the order

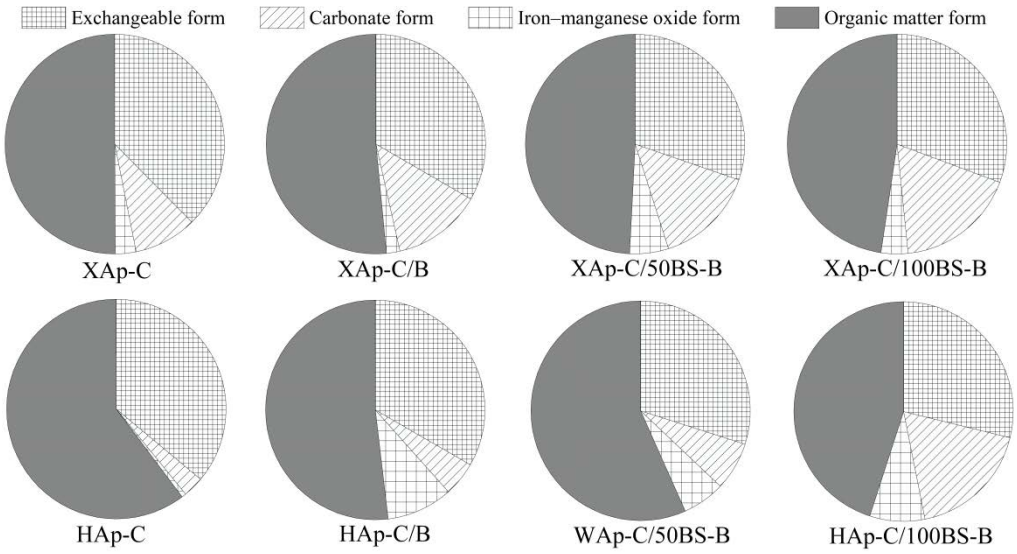

Fig. 4. Distribution of Cu form on different materials.

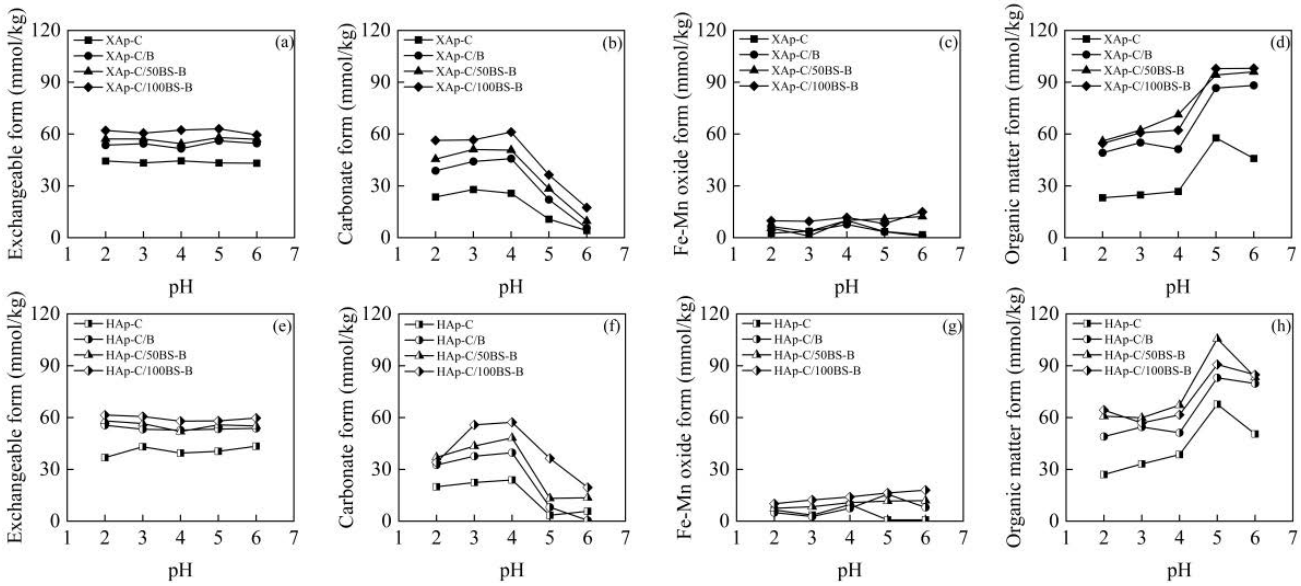

Fig. 5. Effect of pH on Cu content in exchangeable (a and e), carbonate (b and f), Fe–Mn oxide (c and g), and organic matter (d and h) forms.

XAp-C/100BS-B > HAp-C/100BS-B > XAp-C/50BS-B > HAp-C/50BS-B > XAp-C/B > HAp-C/B > XAp-C > HAp-C. With increased pH, the Cu content in organic matter form on each material initially increased and then decreased or stabilized and reached the maximum at pH 5. The content of carbonate Cu initially increased and then decreased with increased pH, reaching the maximum at pH 4 then remarkably decreasing beyond pH 4. The Cu content in exchangeable and Fe–Mn oxide forms adsorbed by the materials had little variation with the change in pH, basically keeping a weak fluctuation trend. These results were primarily due to the effect of pH change on the materials' OH^- and H^+ contents. Increased pH resulted in high OH^- content on the material surface, and Cu in carbonate form can be dissociated in the solution. Cu^{2+} in solution can also easily combine with the organic matter on the material surface, inducing a change in the content of Cu from carbonate form into organic matter form.

3.6. Cycling performance of the tested materials

After the Cu^{2+}-adsorption experiment, XAp-C/100BS-B and HAp-C/100BS-B were regenerated with 5% mass ratio of nitric acid solution with a solid-to-liquid ratio of 1:30 and a regeneration time of 2 h. The mass loss of materials and adsorption amount of Cu^{2+} after three times of regeneration are shown in Fig. 6a and b, respectively. The mass loss of XAp-C/100BS-B and HAp-C/100BS-B reached

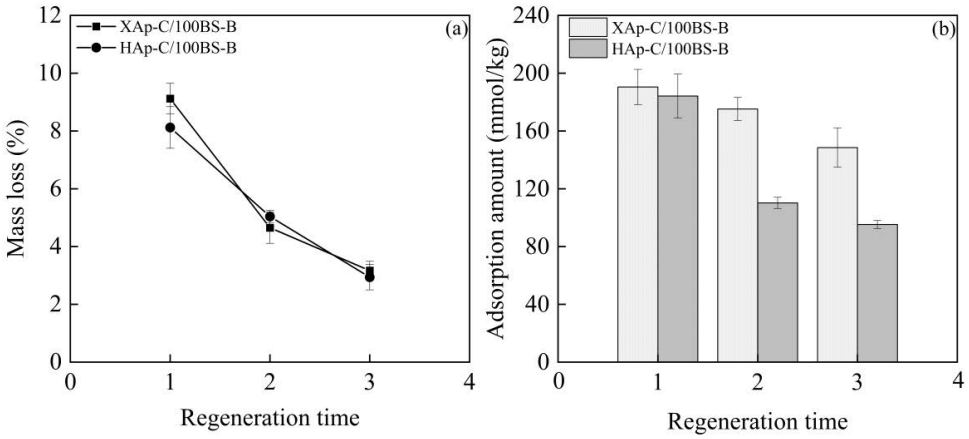

Fig. 6. Regeneration properties of the tested materials.

9.1% and 8.1%, respectively, after the first regeneration. With increased regeneration time, the mass loss of XAp-C/100BS-B and HAp-C/100BS-B gradually decreased, and the loss rate of the third regeneration was only about 3.0%. After one regeneration, the amount of Cu^{2+}-adsorbed onto XAp-C/100BS-B and HAp-C/100BS-B can still reach about 80% of that on the non-regenerated materials. With increased regeneration time, the Cu^{2+} adsorption amount decreased, and the decrease rate on HAp-C/100BS-B was larger than that on XAp-C/100BS-B. XAp-C/100BS-B was a good cyclic-adsorption material whose adsorption effect can still reach 62.6% of the original material after three times of regeneration. The mass loss of the materials during regeneration resulted in reduced BS-B on the surface of Ap-C/BS-B and affected the ion exchange of Cu^{2+}. Conversely, if the material was treated with nitric acid solution many times, the organic matter content on the surface of the materials would be reduced, and the complexation of the materials with Cu^{2+} would be weakened.

4. Discussion

BS-12 has a hydrophobic carbon chain with a positively charged quaternary amine group and a negatively charged carboxyl hydrophilic group at the end. The molecules of BS-12 are bonded with one another by hydrophobic carbon chains and extend outward [24]. When B was modified by BS-12, it easily combined with the negative charge sites on the outer surface of B through the positively charged group $-N^{+}$ end, leaving the negative carboxyl group exposed to adsorb Cu^{2+} and combine new BS-12 molecules. This process was primarily due to electrostatic attraction, which was a physical reaction. B had good ion-exchange capacity, and Cu^{2+} adsorption occurred through ion exchange, which was a chemical endothermic reaction [10]. Ap-C loaded with BS-B can effectively change the surface and internal structure of Ap-C and obtain more active functional groups and adsorption sites [25]. Moreover, Ap-C loaded with BS-B can still directly interact with Cu^{2+} at a low pH, and the effect was significantly enhanced. The Ap-C/BS-B materials can react with Cu^{2+} through electrostatic attraction, surface chelation, surface redox, chemical precipitation, and ion exchange. Thermodynamic parameters showed that the adsorption was a positive temperature effect (chemisorption), and the kinetic parameters also confirmed the chemisorption.

In the Tessier continuous extraction method, Cu in exchangeable, carbonate, Fe–Mn oxide, and organic matter forms are called secondary heavy metals, and they are significantly affected by external environmental factors. Cu in exchangeable form is easily affected by the change in water ion composition; Cu in carbonate form is easily affected by the change in pH; Cu in Fe–Mn oxide form can easily release the adsorbed Cu^{2+} under the reductive condition; and Cu in organic matter form can cause the desorption of Cu^{2+} under the condition of oxidation [26]. The content and percentage of Cu in various forms can characterize the transformation trend among the forms, as well as display the difficulty level of Cu migration and the possibility of secondary pollution in the exchange reaction between solution and materials [27]. The basic physico-chemical properties of the tested materials in Table 1 and the contents of various copper forms adsorbed were linearly fitted, and the results are shown in Table 5. The pH of the materials was moderately correlated with the contents of various Cu forms, whereas the CEC and specific surface area (S_{BET}) were poorly correlated with the contents of various Cu forms. These results showed that the basic physico-chemical properties of the materials were not the key factors determining the adsorption forms of Cu but were correlated with the pH of the materials. Meanwhile, the infrared spectra of the material before and after Cu^{2+} adsorption were compared (Fig. 7). Results showed that the C=O, H–O, and C–H bonds on the materials' surface shifted after Cu^{2+} adsorption, indicating that C=O, H–O, and C–H on the surface were involved in the Cu^{2+} adsorption process. Furthermore, the movement of the peak to a high wavenumber meant that the energy required for vibration was lower and that the group was more stable.

5. Conclusion

- The adsorption isotherms of Cu^{2+} on the tested materials were all L-shaped, consistent with the Langmuir model. q_m on the tested materials changed between 100.82 and

Table 5
Correlations between Cu forms and the physico-chemical properties of materials

Cu form	Physico-chemical properties	Regression equation	r	S
Exchangeable form (E)	pH	pH = –0.029E + 10.37	0.4270	0.53
	CEC	CEC = 1.037E + 137.49	0.1184	72.40
	S_{BET}	S_{BET} = –0.073E + 12.93	0.1465	4.11
Carbonate form (C)	pH	pH = –0.023C + 9.28	0.5541	0.48
	CEC	CEC = –0.786C + 208.56	0.1498	72.09
	S_{BET}	S_{BET} = –0.030C + 9.60	0.0989	4.14
Fe–Mn oxide form (F)	pH	pH = –0.051F + 9.27	0.5579	0.48
	CEC	CEC = –2.513F + 215.06	0.2175	71.16
	S_{BET}	S_{BET} = –0.402F + 12.54	0.6095	3.30
Organic matter form (O)	pH	pH = –0.016O + 10.14	0.4570	0.52
	CEC	CEC = 0.377O + 160.76	0.0885	72.63
	S_{BET}	S_{BET} = –0.075O + 15.42	0.3086	3.96

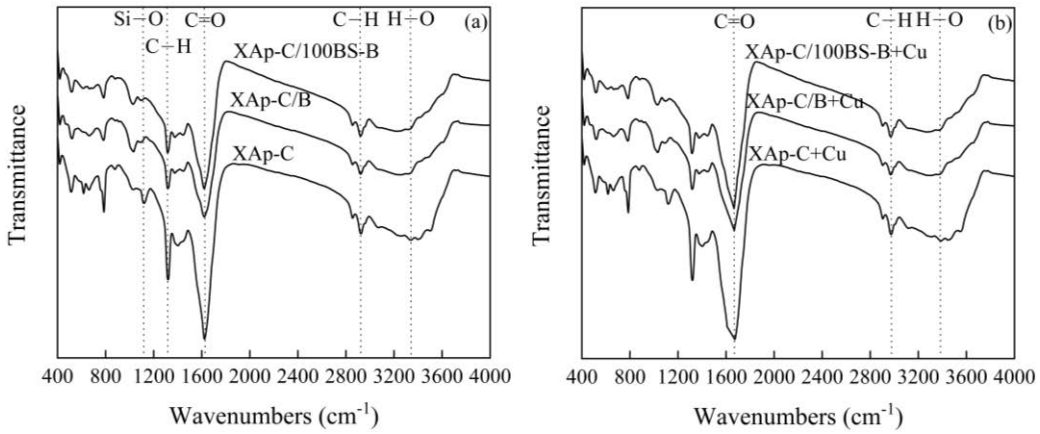

Fig. 7. Fourier-transform infrared spectroscopy characteristics before (a) and after (b) Cu^{2+} adsorption onto the tested materials.

286.31 mmol/kg, Under the same conditions, the amount of Cu^{2+} adsorbed onto XAp-C/BS-B was better than adsorbed onto HAp-C/BS-B, and that adsorbed onto XAp-C/100BS-B was the optimum.

- Thermodynamic parameters showed that Cu^{2+} adsorption was a spontaneous, endothermic, and entropy-ncreasing reaction, Kinetic fitting further showed that Cu^{2+} adsorption conformed to the pseudo-second-order kinetic model.
- Within pH 2–6, the Cu^{2+} adsorption amount initially increased and then decreased, reaching the peak at pH 5. The absorbed Cu on the tested materials was primarily in organic matter and exchangeable forms, followed by the carbonate form and then the Fe–Mn oxide form.
- With increased pH, the carbonate Cu on the materials was gradually transformed into the organic matter form, and Cu in exchangeable and Fe–Mn oxide forms were basically unchanged.

Acknowledgements

The authors wish to acknowledge and thank the Fundamental Research Funds of China West Normal University (20A022; 17E062), the Tianfu Scholar Program of Sichuan Province (2020–17), and the National Natural Science Foundation of P.R. China (41271244).

Conflict of interests

The authors declare that they have no conflict of interest.

References

[1] S.-F. Lim, A.Y.W. Lee, Kinetic study on removal of heavy metal ions from aqueous solution by using soil, Environ. Sci. Pollut. Res. Int., 22 (2015) 10114–10158.
[2] L. Shukla, N. Jain, A review on soil heavy metals contamination: effects, sources and remedies, Appl. Ecol. Environ. Sci., 10 (2022) 15–18.
[3] J. Du, Z. Wang, J. Liu, S. Zhong, C. Wei, Distribution characteristics of soil heavy metals, their source identification and their changes influenced by anthropogenic cultivation activities in purple hilly regions of Sichuan basin, China, J. Soil Sci. Plant Nutr., 20 (2020) 1080–1091.
[4] M.F. Chen, Review on heavy metal remediation technology of soil and groundwater at industrially contaminated site in China, Bull. Chin. Acad. Sci., 29 (2014) 327–335.
[5] M. Ahmad, S.S. Lee, S.E. Lee, M.I. Al-Wabel, D. Tsang, Y.S. Ok, Biochar-induced changes in soil properties affected

immobilization/mobilization of metals/metalloids in contaminated soils, J. Soil Sediment, 17 (2017) 717–730.
[6] Z.H. Huang, Y.Z. Li, W.J. Chen, J.H. Shi, N. Zhang, X.J. Wang, Z. Li, L.Z. Gao, Y.X. Zhang, Modified bentonite adsorption of organic pollutants of dye waste water, Mater. Chem. Phys., 202 (2017) 266–276.
[7] X.D. Jin, H.J. Ma, G.Q. Zeng, H. Wu, Discussion on remediation effect and mechanism of new soil amendment on water-soil compound heavy metal pollution, Environ. Eng., 37 (2019) 17–22.
[8] B. Li, Y.J. Yan, J.Y. Zhang, Y.F. Pan, H.N. Xiao, Z.G. Xuan, Z.H. Huang, Adsorption properties of ethylenediamine modified sawdust for As(V) removal from wastewater, Ion Exch. Adsorpt., 34 (2018) 29–39.
[9] J.X. Yi, Z.P. Huo, M.A. Asiri, K.A. Alamry, J.X. Li, Application of agroforestry waste biomass adsorption materials in water pollution treatment, Prog. Chem., 31 (2019) 760–772.
[10] H. Deng, L. Zhu, D. Wang, L. Ren, W. Li, Effect of modified bentonite on copper migration via bank soils in the Jialing River, Southwest China, Soil Tillage Res., 218 (2022) 105322–105331.
[11] W.B. Li, L. Zhu, H.Y. Deng, Y.F. Zhang, J. Xie, X.Y. Chen, T. Li, Z.F. Meng, Effect of biochar application on adsorption of copper by riverbank soils, Earth Environ., 48 (2020) 250–257.
[12] D.Y. Li, R.J. Yang, H.Y. Luo, S.T. Liu, Y.L. Liu, O. Peng, B.Q. Tie, Effect of adsorption of cadmium from aqueous solution by hexadecyl trimethylammonium bromide modified biochar, Chin. J. Environ. Eng., 13 (2019) 1809– nnooiv b/821.
[13] Y. Qiu, Q. Zhang, M. Li, Z.X. Fan, W.J. Sang, C.F.Y. Xie, D.Y. Niu, Adsorption of Cd(II) from aqueous solutions by modified biochars: comparison of modification methods, Water Air Soil Pollut., 230 (2019) 84–95.
[14] W.B. Li, Z. Liu, Z.F. Meng, S. Ren, S.E. Xu, Y. Zhang, M.Y. Wang, Composite modification mechanism of cationic modifier to amphoteric modified kaolin and its effects on surface characteristics, Int. J. Environ. Sci. Technol., 13 (2016) 2639–2648.
[15] A.S. Han, T. Ahn, Effect of capillary number on the residual saturation of colloidal dispersions stabilized by a zwitterionic surfactant, Appl. Sci., 11 (2021) 524–532.
[16] J. Xie, H.Y. Deng, L. Zhu, Y.F. Zhang, W.B. Li, D. Wang, Z.F. Meng, Preparation of amphoteric modified magnetized carbon and its adsorption to Cu(II), Desal. Water Treat., 194 (2020) 180–186.
[17] S.B. Bu, Z.F. Meng, S. Yek, M.F. Zhang, T. Wang, S. Ren, L.K. Zhang, Adsorption and interaction of Cu^{2+} and Pb^{2+} on BS-12 amphoteric modified bentonites, Environ. Sci., 40 (2019) 4611–4619.
[18] T. Xie, Z.F. Meng, H.Y. Lu, W. Liu, D. Bai, K. Tian, Studies on Cr(VI) and Cd^{2+} adsorption on BS-12+DAS complex modified bentonite, Acta Sci. Circum., 38 (2018) 2833–2841.
[19] K.R. Miriam, L.S. Kate, S. Laura, An appraisal of microwave-assisted Tessier and BCR sequential extraction methods for the analysis of metals in sediments and soils, J. Soil Sediment, 11 (2011) 518–528.
[20] A. Kicińska, R. Pomykaa, M. Izquierdo-Diaz, Changes in soil pH and mobility of heavy metals in contaminated soils, Eur. J. Soil Sci., 6 (2021) 13203–13216.
[21] M.M. Qiao, H.B. Ji, X.F. Zhu, Y. Chen, Fraction distribution and risk assessment of heavy metals in sediments of inflow rivers of Miyun Reservoir, Acta Sci. Circum., 33 (2013) 3324–3333.
[22] Z.F. Meng, N. Gong, R.H. Li, Z.Q. Zhang, Y.P. Zhang, Adsorption of aniline on an organic modified Lou soil, Chin. J. Soil Sci., 39 (2008) 143–149.
[23] K. Kadirvelu, M. Kavipriya, C. Karthika, N. Vennilamani, S. Pattabhi, Mercury(II) adsorption by activated carbon made from sago waste, Carbon, 42 (2004) 745–752.
[24] X.L. Li, W.B. Li, H.Y. Deng, T. Li, D. Wang, Enhanced adsorption of Cu^{2+} on purple soil by amphoteric-modified materials, Desal. Water Treat., 196 (2020) 150–158.
[25] J.Y. Liu, G.H. Huang, J.Q. Deng, K. Liu, Y.B. Xie, Adsorbent prepared from waste pomelo peel and its adsorption of Pb^{2+} in wastewater, J. Ecol. Rural Environ., 28 (2012) 187–191.
[26] Q. Liang, H.Y. Deng, W.B. Li, X.L. Hu, Y. Yang, Effect of coexistence of BS-12 on the adsorption stability and morphology of copper in coastal soil, Fresenius Environ. Bull., 29 (2020) 9429–9437.
[27] X.L. Zhong, S.L. Zhou, M.L. Huang, Q.G. Zhao, Chemical form distribution characteristic of soil heavy metals and its influencing factors, Ecol. Environ. Sci., 18 (2009) 1266–1273.